

Floquet-engineering the exceptional points in parity-time-symmetric magnonics

Xi-guang Wang¹, Lu-lu Zeng¹, Guang-hua Guo¹, Jamal Berakdar^{2*}

¹ *School of Physics and Electronics,*

Central South University, Changsha 410083, China

² *Institut für Physik, Martin-Luther Universität*

Halle-Wittenberg, 06099 Halle/Saale, Germany

* *email: jamal.berakdar@physik.uni-halle.de*

(Dated: October 17, 2023)

arXiv:2310.09300v1 [cond-mat.mes-hall] 8 Oct 2023

Abstract

Magnons serve as a testing ground for fundamental aspects of Hermitian and non-Hermitian wave mechanics and are of high relevance for information technology. This study presents setups for realizing spatio-temporally driven parity-time (PT) symmetric magnonics based on coupled magnetic waveguides and magnonic crystals. A charge current in a metal layer with strong spin-orbit coupling sandwiched between two insulating magnetic waveguides leads to gain or loss in the magnon amplitude depending on the directions of the magnetization and the charge currents. When gain in one wave guide is balanced by loss in the other waveguide a PT-symmetric system hosting non-Hermitian degeneracies (or exceptional points (EPs)) is realized. For AC current multiple EPs appear for a certain gain/loss strength and mark the boundaries between the preserved PT-symmetry and the broken PT-symmetry phases. The number of islands of broken PT-symmetry phases and their extensions is tunable by the frequency and the strength of the spacer current. At EP and beyond, the induced and amplified magnetization oscillations are strong and self-sustained. In particular, these magnetization auto-oscillations in broken PT-symmetry phase occur at low current densities and do not require further adjustments such as tilt angle between electric polarization and equilibrium magnetization direction in spin-torque oscillators, pointing to a new design of these oscillators and their utilization in computing and sensoric. It is also shown how the periodic gain/loss mechanism allows for the generation of high-frequency spin waves with low-frequency currents. For spatially-periodic gain/loss acting on a magnonic crystal, magnon modes approaching each other at the Brillouin-zone boundaries are highly susceptible to PT-symmetry, allowing for a wave-vector-resolved experimental realization at very low currents.

Introduction: Long-wave length elementary excitations around a magnetically ordered stable state in an extended system are spin waves (SW) or magnons (in reference to their excitation quanta). SWs can be geometrically and magneto-statically (finite-size) quantized and steered by a variety of external probes such as magnetic and electric fields as well as by charge currents or temperature gradients.[1–5] Thus, SWs are well suited for use in (classical) information transfer and processing.[6, 7] Basic hardware elements for magnonic data channeling and processing are thereby coupled magnonic waveguides (WGs), meaning magnetically ordered stripes that exchange power via coupling mediated by dipolar fields, or Rudermann-Kittel-Kasuya-Yosida (RKKY) interaction.[8–11]

Intrinsic magnetic damping may compromise the fidelity of information and cause power dissipation. A way to act on magnetic damping externally is offered by spin-orbit torque (SOT), which arises when the WG is attached to a metallic (such as Pt) layer with strong spin orbit coupling.[5, 12–14] The magnetic damping strength α in the WG is then controlled by a DC bias on the metallic layer that drives a charge current density \mathbf{J}_{Pt} . The mechanism behind this effect is in short: an interfacial spin dependent scattering generates spin accumulations \mathbf{A} at the interfaces of the WG/metallic layer, the strength of which is set by the spin Hall angle. The spin accumulations act with a torque (spin orbit torque (SOT)) on the magnetization density \mathbf{m} . The torque direction is set by the charge current density and magnetization vectors. Flipping the direction of \mathbf{m} or \mathbf{J}_{Pt} changes the sign of \mathbf{T} . As for the SWs dynamics, SOT has a field-like and damping/antidamping-type effects. It is possible to realize a situation where the metallic layer is sandwiched between two coupled magnonic WGs resulting in damping (magnonic loss) in one WG and antidamping (magnonic gain) in the other WG.[15–19] This is a typical situation of gain/loss setup, as discussed in connection with parity-time (PT) symmetric systems [15, 17, 18, 20–37] which have been investigated in optics[23–27], acoustics[28, 29], electronics[30, 31] and spintronic[15–19, 32–37]. Indeed, it is demonstrated mathematically [15], how the dynamics in coupled gain/loss magnonic WGs (the system studied here) can be mapped to PT-symmetric non-Hermitian Hamiltonian. Such system can be driven externally to the non-Hermitian degeneracy, or exceptional point (EP) by changing SOT, meaning J_{Pt} .

EP can be viewed as a separation point between the PT symmetry broken/or preserving phases [17, 23–25, 27, 38–42]. Approaching the EP, different eigenmodes collapse changing significantly the mode propagations. Above the EP, in the PT-symmetry-broken phase, the mode propagation can be amplified (attenuated) under gain (loss). These special features can be exploited for designing new types of devices for information processing and for sensoric. Experimentally, the existence of EP has been validated in two coupled magnets with different damping [36], and where the damping is imparted by laser pulses [43].

So far, gain and loss in magnon amplitude were considered to be homogeneous in time and space across the magnonic WGs. In the present work, we show that PT-symmetric magnonic WGs with time or/and space-varying gain and loss show qualitatively new features that are of direct relevance for applications. As sketched in Fig.1, such systems can be fabricated by nanostructuring the Pt layer or by a time-dependent voltage which drives

then a time-dependent J_{Pt} . An appropriate framework for analyzing the dynamics in these cases is the Floquet or the Bloch-state approach applied to PT-symmetric non-Hermitian dynamics. Performing the analysis, we identify multiple EPs from Floquet quasienergies where magnon amplification is induced.

Comparing with a constant magnonic gain and loss, the charge current densities needed to approach the EPs are much smaller, and are tunable with the time period of J_{Pt} . For space periodic gain and loss, EP's J_{Pt} becomes very low (compared to typical current densities needed to reach EP in homogeneous PT-symmetric systems [15] or to induce magnetic switching/oscillation) when two magnon modes approach each other, which typically occurs when folding modes at the Brillouin-zone (BZ) boundaries. In contrast to WGs with homogeneous gain/loss, where spin reversal above EP occurs, in our case magnon amplification around the EPs leads eventually to self-sustained oscillation. Recalling the well-documented case of SOT induced magnetization auto-oscillation which depends on the tilt angle between the electric polarization and the equilibrium magnetization direction [44–47], our finding points to a new way for realizing SOT oscillators without tilt-angle adjustments and with the high sensitivity to external probes akin to systems with EPs [19].

Model: The considered magnonic PT-symmetric coupled WGs with time-periodic gain/loss is illustrated in Fig. 1. Two insulating magnetic layers are initially magnetized along $+y$ direction and coupled, via the RKKY interaction that acts through a spacer (Fig. 1(a)). Due to the spin Hall effect, a time-varying charge current in the spacer results in SOTs $\mathbf{T}_{1(2)} = \gamma c_J \mathbf{m}_{1(2)} \times (\pm \mathbf{y}) \times \mathbf{m}_{1(2)}$. [12–14] The coupled (linear and nonlinear) magnetic dynamics is governed by Landau-Lifshitz-Gilbert (LLG) equations,

$$\frac{\partial \mathbf{m}_p}{\partial t} = -\gamma \mathbf{m}_p \times \mathbf{H}_{\text{eff},p} + \alpha \mathbf{m}_p \times \frac{\partial \mathbf{m}_p}{\partial t} + \mathbf{T}_p, \quad (1)$$

$p = 1, 2$ enumerate WG1 and WG2. γ is the gyromagnetic ratio, and α is the intrinsic Gilbert damping. The effective field $\mathbf{H}_{\text{eff},p} = \frac{2A_{\text{ex}}}{\mu_0 M_s} \nabla^2 \mathbf{m}_p + \frac{J_F}{\mu_0 M_s t_p} \mathbf{m}_{p'} + H_0 \mathbf{y}$ consists of the internal exchange field (with an exchange constant A_{ex}), the RKKY interlayer coupling field (with a coupling constant J_F), and the external field H_0 . M_s is the saturation magnetization. $p, p' = 1, 2$ and $p \neq p'$. t_p is the p th layer thickness and μ_0 is the vacuum permeability. The SOT strength coefficient $c_J = \frac{S \theta_{\text{SH}} \hbar J_{Pt}}{2 \mu_0 e t_p M_s}$ is proportional to the charge current density J_{Pt} , the spin-Hall angle θ_{SH} of the spacer, and the WG/spacer interface transparency S .

In numerical calculations, we adopt the following parameters for Yttrium–Iron–Garnet

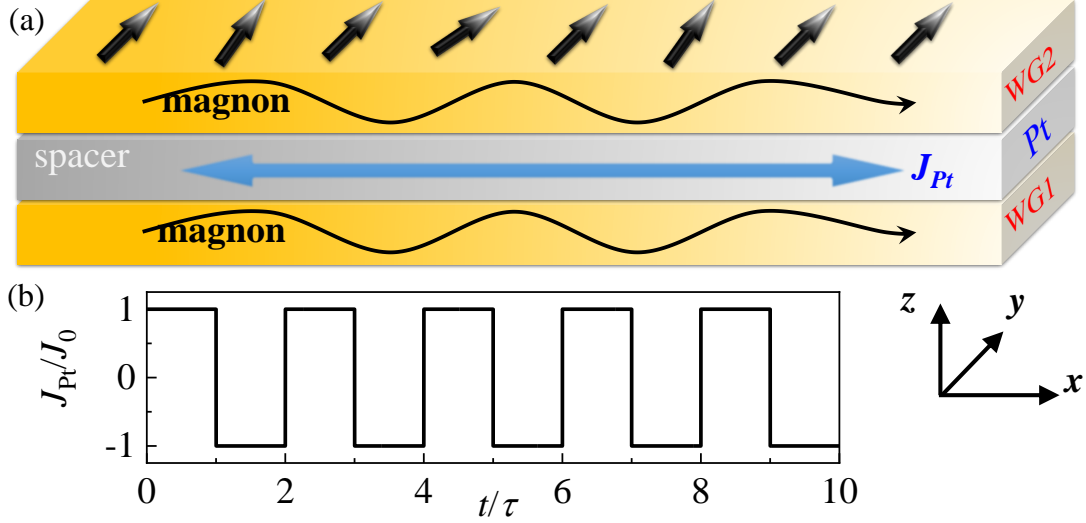


FIG. 1. (a) Schematic of the RKKY-coupled magnonic waveguides with time-periodic PT symmetry. Two magnetic films serve as the magnon waveguides (WG1 and WG2) and are coupled ferromagnetically by a nanoscale conductive spacer (for instance Pt) with a spin Hall angle. Injecting into the spacer a time-varying charge current J_{Pt} results in opposite spin-orbit torques (SOTs) acting on the magnetic dynamics in WG1 and WG2 and leading to time-varying magnonic gain/loss in WG1/WG2. (b) The time-periodic current J_{Pt} with period $T = 2\tau$ used in the simulations.

(YIG): saturation magnetization $M_s = 1.4 \times 10^5$ A/m, exchange constant $A_{ex} = 3 \times 10^{-12}$ J/m. The Gilbert damping α can be experimentally varied within a wide range via material engineering [48] ($\alpha = (6.15 \pm 1.5) \times 10^{-5}$ is reported in [49]), below we use $\alpha = 0.004$. The interlayer exchange constant is $J_F = 9 \times 10^{-5}$ J/m², and the exchange field amplitude is $\frac{J_F}{\mu_0 M_s t_p} \approx 1 \times 10^5$ A/m with $t_p = 4$ nm. A sufficiently strong magnetic field $H_0 = 2 \times 10^5$ A/m is applied along the $+y$ (or $+x$) direction to drive the WGs to the saturated state.

We will perform full-fledged numerical simulations and to analyze the numerical results in certain regimes, we setup a linearized analytical model. For analytical modeling we consider small deviations of $\mathbf{m}_{s,p} = (\delta m_{x,p}, 0, \delta m_{z,p})$ around the equilibrium $\mathbf{m}_{0,p} = \mathbf{y}$. Defining $\psi_p = \delta m_{x,p} + i\delta m_{z,p}$, we deduce the coupled SW equation under the linear assumption ($\|\mathbf{m}_{s,p}\| \ll 1$),

$$\begin{aligned} i\frac{\partial\psi_1}{\partial t} - [(\omega_0 - \alpha\omega_{J,t}(t)) - i(\omega_J + \alpha\omega_0)]\psi_1 + q\psi_2 &= 0, \\ i\frac{\partial\psi_2}{\partial t} - [(\omega_0 + \alpha\omega_{J,t}(t)) + i(\omega_J - \alpha\omega_0)]\psi_2 + q\psi_1 &= 0. \end{aligned} \quad (2)$$

The WG dispersion of the intrinsic frequency ω_0 with respect to the wave vector k_x reads

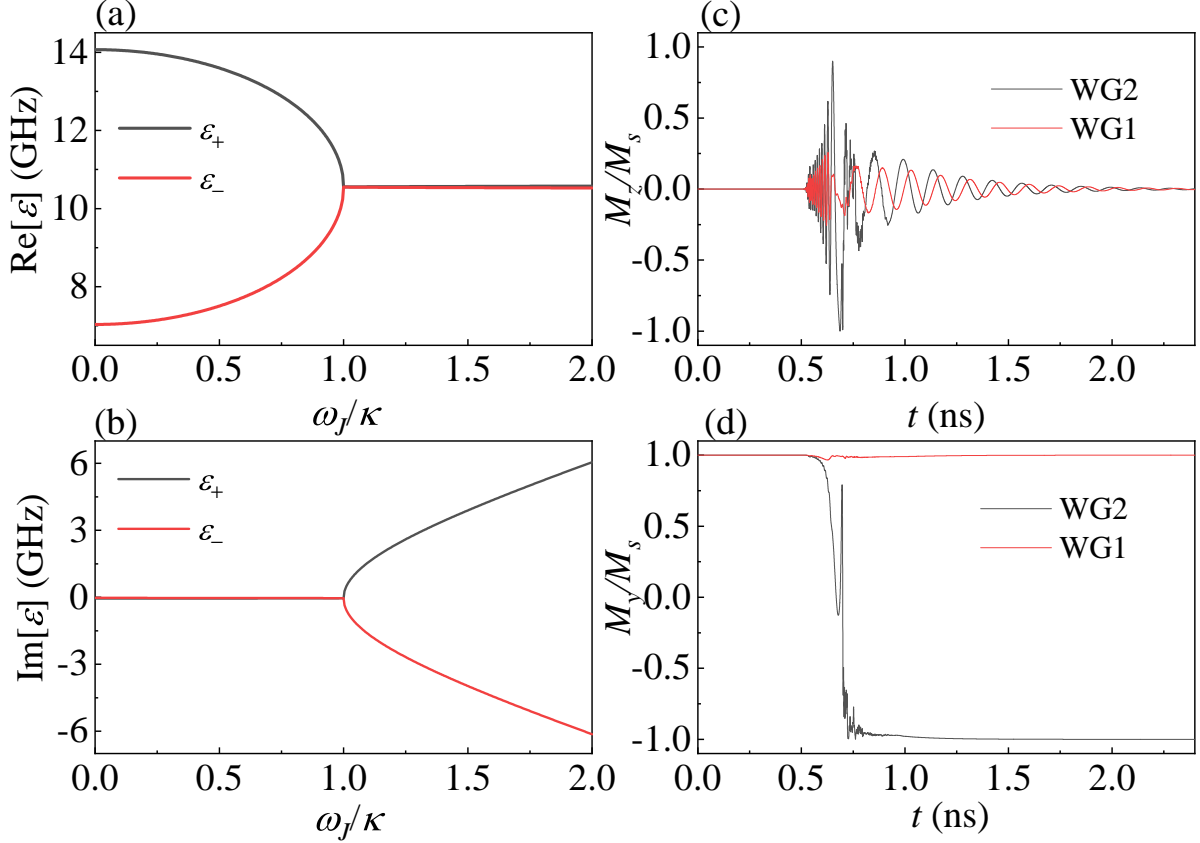


FIG. 2. (a) real and (b) imaginary parts of quasienergies ϵ_{\pm} (Eq. (5)) as functions of SOT coupling strength ω_J at $k_x = 0$ and constant current in the spacer. For $\omega_J/\kappa = 1.1$, time-dependent M_z (c) and M_y (d) at $x = 2000$ nm in WG1 and WG2 (obtained from the numerical simulation based on Eq. (1)). Spin waves are excited by sinc pulse $h(t) = h_a \mathbf{z} \sin(\omega_F t)/(\omega_F t)$ with amplitude $h_a = 1 \times 10^5$ A/m and frequency range 50 GHz applied locally to the region $x = 0$.

$\omega_0(k_x) = \frac{\gamma}{1+\alpha^2} (H_0 + \frac{2A_{\text{ex}}}{\mu_0 M_s} k_x^2 + \frac{J_F}{\mu_0 M_s t_p})$, the time-dependent SOT term related to the gain-loss mechanism is $\omega_{J,t}(t) = \frac{\gamma c_J(t)}{1+\alpha^2}$, and the RKKY-related (static) coupling term is $q = (1 - i\alpha)\kappa$ with $\kappa = \frac{\gamma J_F}{(1+\alpha^2)\mu_0 M_s t_p}$. With the Hall angle $\theta_{\text{SH}} = 0.06$ and interface transparency $S = 0.25$, the value of $\omega_J = \kappa$ corresponds to a charge current density of $J_e = 9 \times 10^8$ A/cm².

Results: When the bias voltage on the spacer is alternating with period T , we have $\omega_{J,t}(t + T) = \omega_{J,t}(t)$. For clarity we study a simple periodic step-function with alternating polarity (cf. Fig.1(b)) such that if $\omega_{J,t}(0 \leq t \leq \tau) = \omega_J$ and $\omega_{J,t}(\tau \leq t \leq T) = -\omega_J$. Thus, $T = 2\tau$. We consider the case where the gain compensates for the loss (meaning the two WGs are of the same material). Preparing the system to be in the state (ψ_1^0, ψ_2^0) , and

starting with positive (negative) SOT polarity from Eq. (2), the evolved state after time τ reads

$$\begin{pmatrix} \psi_1 \\ \psi_2 \end{pmatrix} = \hat{M}_{\text{P(N)}}(\tau) \begin{pmatrix} \psi_1^0 \\ \psi_2^0 \end{pmatrix}. \quad (3)$$

For positive (negative) ω_J we have

$$\begin{aligned} M_{\text{P}} &= \frac{e^{-i\omega_e}}{2d} \begin{pmatrix} e^{-id_e}(d - i\omega_J) + e^{id_e}(d + i\omega_J) & (e^{id_e} - e^{-id_e})\kappa \\ (e^{id_e} - e^{-id_e})\kappa & e^{-id_e}(d + i\omega_J) + e^{id_e}(d - i\omega_J) \end{pmatrix}, \\ M_{\text{N}} &= \frac{e^{-i\omega_e}}{2d} \begin{pmatrix} e^{-id_e}(d + i\omega_J) + e^{id_e}(d - i\omega_J) & (e^{id_e} - e^{-id_e})\kappa \\ (e^{id_e} - e^{-id_e})\kappa & e^{-id_e}(d - i\omega_J) + e^{id_e}(d + i\omega_J) \end{pmatrix}. \end{aligned} \quad (4)$$

With the spacer current angular frequency $\omega_{\text{F}} = \pi/\tau$, we introduced $d = \sqrt{\kappa^2 - \omega_J^2}$, $\omega_e = \pi(1 - i\alpha)\omega_0/\omega_{\text{F}}$, $d_e = \pi(1 - i\alpha)d/\omega_{\text{F}}$. The combined propagation matrix after one period is $\hat{M}(T) = \hat{M}_{\text{P}}(\tau)\hat{M}_{\text{N}}(\tau)$. For periodic driving, Floquet's theorem states for solutions $e^{-i\epsilon_{\pm}t}\phi_{\pm}(t)$ that the function (Floquet state) $\phi_{\pm}(t) = \phi_{\pm}(t + T)$, and the Floquet's quasienergy $\epsilon_{\pm} \in [0, \omega_{\text{F}}]$ defined up to multiples of ω_{F} .

At first, we analyze the case with constant SOT, i.e., $\tau \rightarrow \infty$. Depending on the sign of ω_J , the evolution follows $\hat{M}_{\text{P}}(t)$ or $\hat{M}_{\text{N}}(t)$, and from the eigenvalues V_{\pm} of the matrices we can obtain the complex Floquet quasienergies as

$$\epsilon_{\pm} = (1 - i\alpha)(\omega_0 \pm d). \quad (5)$$

For the constant SOT, these quasienergies are exactly the same as the eigen-frequencies (optic and acoustic modes) of the coupled waveguides with level spacing $\omega_{\text{d}} := 2d(1 - i\alpha)$. [15] If $\omega_J \rightarrow \kappa$, then $d \rightarrow 0$ and the two modes coincide (Fig. 2(a-b)) signaling the occurrence of a non-Hermitian degeneracy point (EP) that separates the PT-symmetry preserved and broken phases. Besides, the system becomes unstable when the imaginary part of ϵ_+ becomes positive (for $\omega_J > \kappa$), i.e., $0 \leq |d| - \alpha\omega_0$. Under a very small damping, the critical value for driving the instability is set by EP. A non-vanishing α shifts the instability slightly above the EP. Here, the unstable and stable regions are separated by the line $\omega_J = \kappa$ (for the small $\alpha = 0.004$). Above the critical value (say at $\omega_J = 1.1\kappa$), we simulate the time-dependent magnetization of WG1 and WG2. As shown in Fig. 2(c-d), the magnetization oscillation is quickly amplified at the beginning. The amplified oscillation renders the equilibrium magnetization of WG2 switched to the $-y$ direction. Then, the oscillation is soon damped.

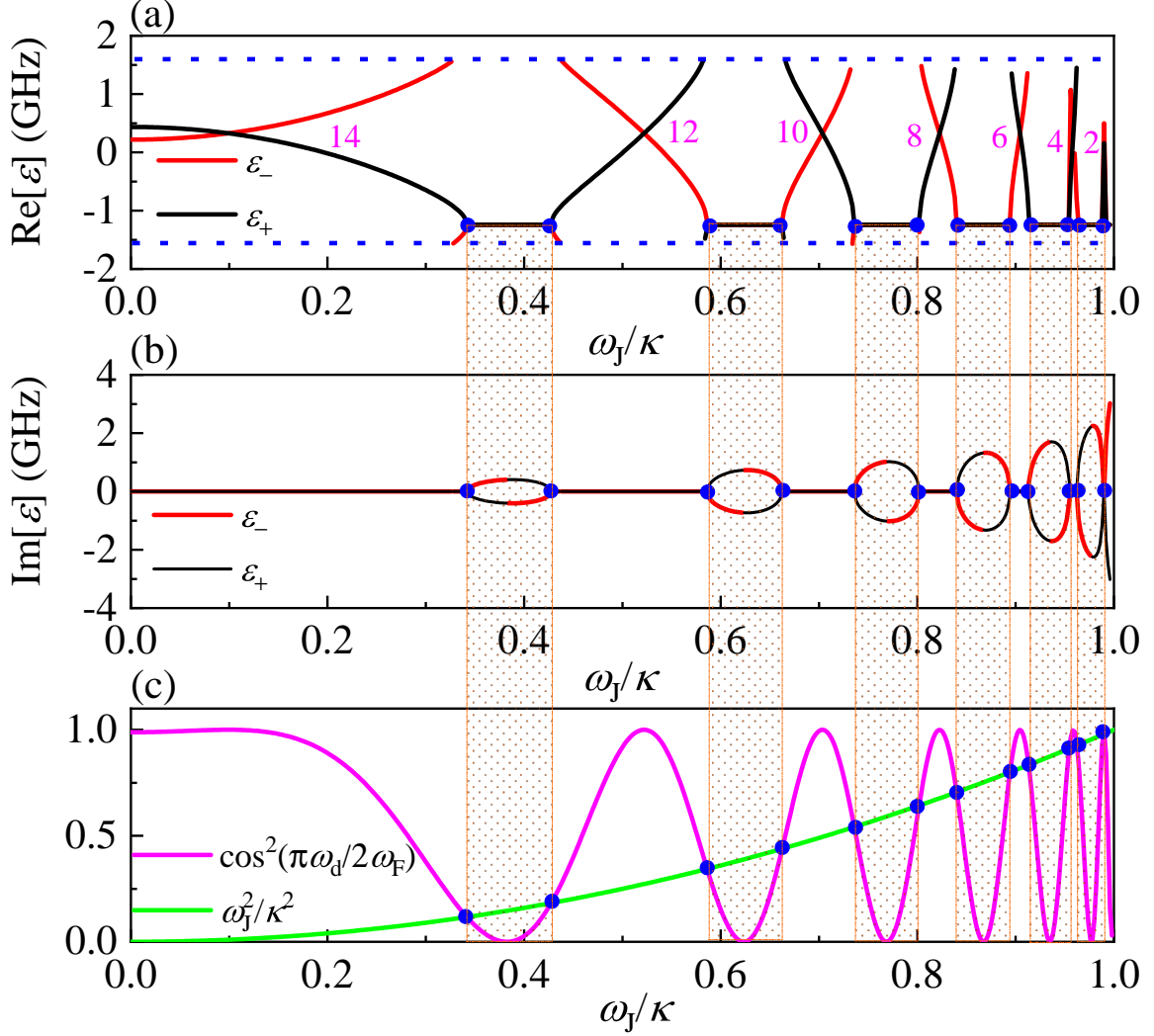


FIG. 3. (a) real and (b) imaginary parts of Floquet quasienergies ϵ_{\pm} (Eq. (7)) as functions of the amplitude ω_J of periodic SOT with angular frequency $\omega_F = \pi$ GHz and $k_x = 0$ for $\alpha \rightarrow 0$. Real parts of ϵ_{\pm} in the zone $-\omega_F/2$ and $\omega_F/2$ (marked by blue dashed lines) with $T = 2\pi/\omega_F$ being the AC charge current period. The integers (14, 12,...) in (a) are the ratio $\frac{\omega_d}{\omega_F}$ when ϵ_{\pm} cross. (c) $\frac{\omega_J^2}{\kappa^2}$ and $\cos^2(\frac{\pi}{2} \frac{\omega_d}{\omega_F})$ in Eq. (7). Blue full dots mark Floquet EPs conditions. Shaded areas mark the range of broken PT-symmetry phases. Note, the extension and the number of the broken PT-symmetry islands are controllable by the charge current density ($\propto \omega_J$) and frequency (ω_F).

Enhanced oscillation amplitude invalidates the linear assumption necessitating full numerical treatment, see Supplementary Information (SM). [50]

For the time-periodic SOT, the two complex quasienergies are deduced as

$$\epsilon_{\pm} = -\ln \left\{ \frac{e^{-2iw_e}}{2d^2} [(e^{-2id_e} + e^{2id_e})\kappa^2 - 2\omega_J^2 \pm 2\kappa \sinh(id_e)[2(\kappa^2 + \kappa^2 \cosh(2id_e) - 2\omega_J^2)]^{1/2}] \right\} \omega_F / (2\pi i). \quad (6)$$

For small damping ($\alpha \rightarrow 0$), ϵ_{\pm} simplify to

$$\epsilon_{\pm} = -\ln \left\{ \frac{e^{-2iw_e} \kappa^2}{d^2} \left[\cos\left(\frac{\pi\omega_d}{\omega_F}\right) - \frac{\omega_J^2}{\kappa^2} \pm 2i \sin\left(\frac{\pi\omega_d}{2\omega_F}\right) \left[\cos^2\left(\frac{\pi\omega_d}{2\omega_F}\right) - \frac{\omega_J^2}{\kappa^2} \right]^{1/2} \right] \right\} \frac{\omega_F}{2\pi i}. \quad (7)$$

Following current-tunable cases are identified:

- a) When the frequency ω_F and amplitude ω_J of the driving current are such that $\cos^2(\frac{\pi\omega_d}{2\omega_F}) > \frac{\omega_J^2}{\kappa^2}$, the quasienergies ϵ_{\pm} are real and different, indicating a PT-symmetry preserved phase.
- b) Even in this phase, Floquet states may become degenerate when the level spacing is a multiple of the driving frequency, i.e., $\omega_d = 2n\omega_F$ and n is an integer which resembles the standard multiphoton resonance for weak driving [51] and is depicted on Fig.3(a).
- c) At $\cos^2(\frac{\pi\omega_d}{2\omega_F}) = \frac{\omega_J^2}{\kappa^2}$ the modes coalesce signaling EPs in Floquet modes (called henceforth FEPs).
- d) Above the FEP ($\cos^2(\frac{\pi\omega_d}{2\omega_F}) < \frac{\omega_J^2}{\kappa^2}$), ϵ_{\pm} turn complex with the two real parts of ϵ_{\pm} being degenerate, and the two imaginary parts are different which is indicative of the broken PT-symmetry phase. Since $\frac{\omega_J^2}{\kappa^2}$ is monotonous but $\cos^2(\frac{\pi\omega_d}{2\omega_F})$ periodic in ω_J , as we vary the current spacer strength (varying thus ω_J), several broken PT-symmetry islands appear (shaded areas in Fig.3). FEPs mark the boundaries of these islands.

Numerical calculations (Fig. 3) based on Eq. (7) prove the cases a)-c). Importantly, the values of FEPs occur at much smaller ω_J (which is proportional to the current density) as the conventional EP (at $\omega_J = \kappa$), with the first FEP arising at $\omega_J = 0.34\kappa$. For small damping $\alpha = 2 \times 10^{-5}$, α -induced differences in ϵ_{\pm} are negligible, (see calculations in SM [50]). In the PT-symmetry preserved case, the quasienergies ϵ_{\pm} satisfy as usual $\epsilon_{\pm} = \epsilon_{\pm} \pm n\omega_F$, with $n = 0, \pm 1, \dots$ (see Fig. 3). For larger damping, e.g. $\alpha = 0.004$, in the broken PT-symmetry phase small gaps appear between the real parts, and two $\text{Re}[\epsilon_{\pm}]$ coalesce only at the center, and two imaginary parts $\text{Im}[\epsilon_{\pm}]$ are more separated there. Besides, the damping brings in a finite $\text{Im}[\epsilon_{\pm}]$ outside the broken PT-symmetry phases. These larger finite damping induced features make the FEPs not as clear as for small damping, still we can identify the FEPs regions and broken PT-symmetry phase from the region with more separated $\text{Im}[\epsilon_{\pm}]$.

Varying charge current strength (meaning gain/loss strength) the stability behavior can be controlled. Around FEPs (below $\omega_J = \kappa$), the imaginary parts turn positive, indicating

driven instability, i.e., large-amplitude magnetization dynamics. E.g., for $\omega_J/\kappa = 0.388$ in the instability range, the enhanced magnetization oscillation is shown in Fig. 4(c-d). In contrast to a time-constant current ($\omega_F \rightarrow 0$), the enhanced magnetization oscillation persists long after reaching the maximal amplitude. For the range with stable oscillation (say $80\text{ns} < t < 100\text{ns}$), we show the frequency spectrum (see the inset of Fig. 4(d)). Mainly two resonance frequencies are excited, corresponding to the $k_x = 0$ mode of the in-phase acoustic oscillation and the out-of-phase optic oscillation in the coupled WG1 and WG2. Importantly, the excited resonance frequencies differ from the frequency of the spacer current (0.5 GHz) offering so a new method to generate high frequency magnons by an electric current with a very low frequency. Furthermore, we calculate the $k_x - \omega_J$ (at $\tau = 1\text{ns}$) and $\tau - \omega_J$ (at $k_x = 0$) stability diagram (Fig. 4(e-f)). For low k_x , several instability islands are substantial in size; all areas shrink with increasing k_x . For smaller current period T the separated instability areas can be enlarged. Important for a possible experimental realization, to drive the auto-oscillation inside the instability islands with broken PT-symmetry phase, the required precision in T is lower for the larger SOT amplitude ω_J . For example, in our estimation, to drive the instability, the smallest SOT amplitude is $\omega_J/\kappa = 0.03$, which requires the time period $T = (14.2 \pm 0.2) \times 10^{-11}$ s, i.e., the precision is around 2 ps. $\omega_J/\kappa = 0.1$ allows for $T = (14.2 \pm 1) \times 10^{-11}$ s, and larger $\omega_J/\kappa = 0.2$ has $T = (14.6 \pm 2) \times 10^{-11}$ s, indicating lower and lower precession requirement.

For comparison, we also apply constant and periodic SOT to a single waveguide. We consider the SOT $\mathbf{T} = \gamma c_J \mathbf{m} \times (-\mathbf{y}) \times \mathbf{m}$ and the equilibrium stable magnetization $\mathbf{m}_0 = \mathbf{y}$. Following the same procedure discussed above, the quasienergy for constant ω_J in a single WG is $(1 - i\alpha)(\omega_0 + i\omega_J)$. When the antidamping SOT counteracts the damping torque, the imaginary value $\omega_J - \alpha\omega_0 > 0$, and the equilibrium magnetization $\mathbf{m}_0 = \mathbf{y}$ loses its stability. The conclusion agrees well with SOT-induced magnetization oscillation. But the induced oscillation is not sustained. The magnetization is soon reversed to $-y$ and the oscillation is damped. This is in line with studies showing that a sustained auto-oscillation requires a finite tilt angle between the electric polarization and the equilibrium magnetization directions.[44–47] For periodic ω_J in a single WG, the quasienergy becomes $(1 - i\alpha)\omega_0$, which is independent of the amplitude of ω_J . The reason behind this is that the opposite SOT effects from two half periods are completely neutralized. Besides, the above periodic varying SOT is realized in the time domain. In the SM [50], we also analyze a spatially-periodic gain and loss driven

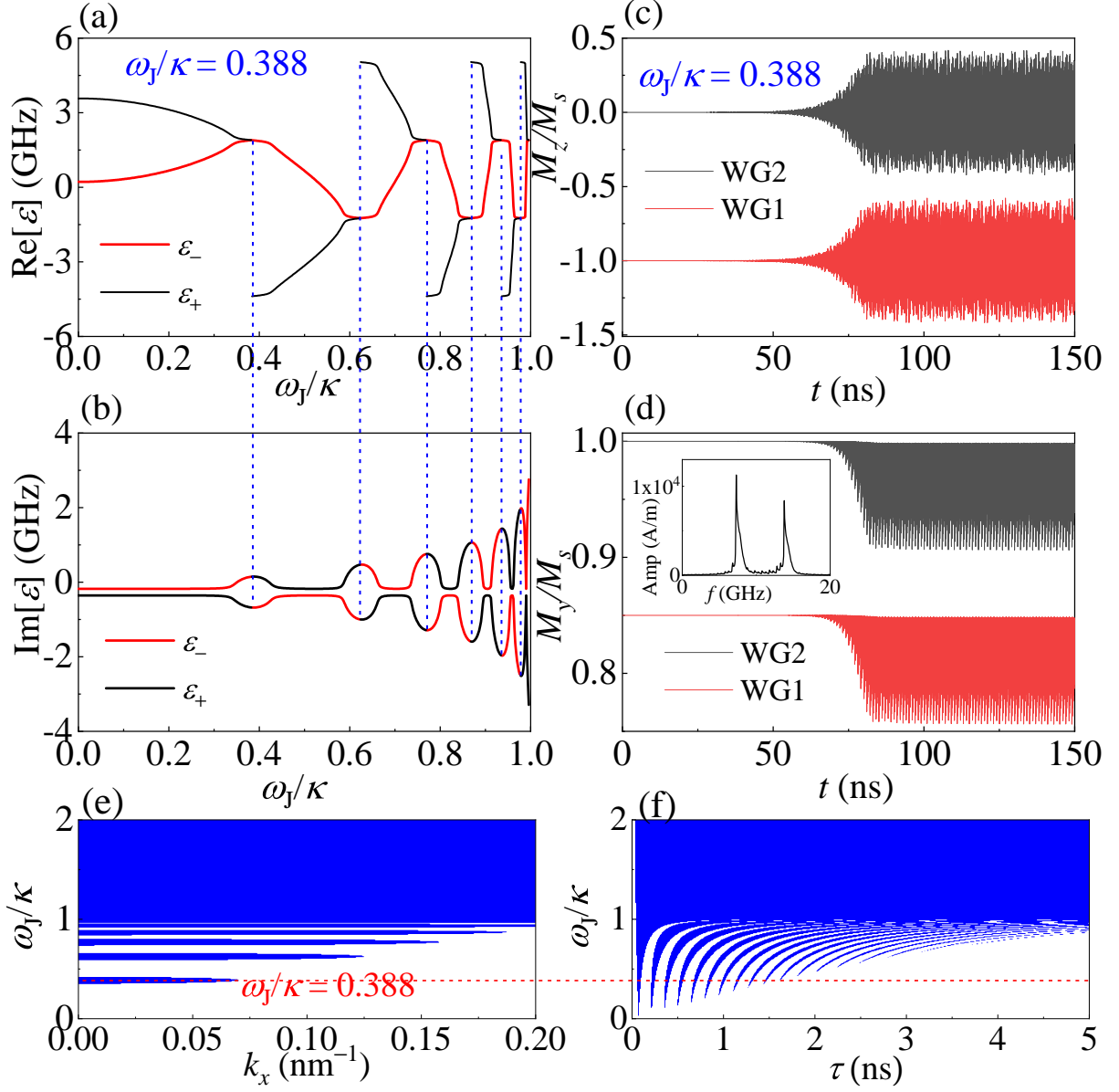


FIG. 4. For the periodic SOT term ω_J (with amplitude ω_J) and $\alpha = 0.004$, (a) real and (b) imaginary parts of quasienergies ϵ_{\pm} (Eq. (6)) as functions of the amplitude ω_J with the period parameter $\tau = 1$ ns and $k_x = 0$. When $\omega_J/\kappa = 0.388$ (inside the instability range), time-dependent (c) $M_z(x = 2000\text{nm})$ and (d) averaged M_y in WG1 and WG2 (obtained from the numerical simulation based on Eq. (1)). A sinc pulse is applied, meaning $h(t) = h_a \mathbf{z} \sin(\omega_F t)/(\omega_F t)$ with the amplitude $h_a = 1 \times 10^5$ A/m and frequency range of 50 GHz, acting locally on the region $x = 0$. The inset in (d) is the frequency spectrum of the magnetization oscillation in last 20 ns. The red curves (WG1) are in the same range with WG2 curves, which are intentionally offset for clarity. (e-f) The stability phase diagram on the (e) $k_x - \omega_J$ space with $\tau = 1$ ns, and (f) $\tau - \omega_J$ space with $k_x = 0$. The shaded region corresponds to the unstable oscillation.

by SOT. As the spin-wave also experiences periodically varying gain and loss during the propagation, we identify lower EPs and auto-oscillation in the broken PT-symmetry phase above EP. Our investigation of a system with coupled periodic loss/more-loss mechanism (SM [50]) also uncovers similar features of EP, demonstrating the versatility of magnonics when combined with PT-symmetry.

Conclusions: We proposed, simulated and analyzed the magnonic dynamics in time-dependent or space-dependent periodic PT-symmetric environment. We identify typical PT-symmetry phenomena. Via the period and the amplitude of driving fields, EPs and instability threshold can be controlled. Different from the case with a homogeneous gain/loss, in the instability region the induced magnetization oscillation is strong and self-sustained, which constitutes a new effective way for realizing magnetization auto-oscillation without the need for a tilt angle in the electric polarization with respect to the equilibrium magnetization direction in a single waveguide. This finding can be used for designing SOT oscillators. For the spatially-periodic case, EP can be reached at small SOTs or charge currents when two modes approach each other which can be achieved via an appropriate modulation of the magnonic crystal. The electric and magnetic non-linear response at EP points to a new type of electrically manipulable Floquet magnonic metamaterials.

Acknowledgements: This work was supported by the DFG through SFB TRR227, and Project Nr. 465098690, the National Natural Science Foundation of China (Grants No. 12174452, No. 12074437, No. 11704415, and No. 11674400), and the Natural Science Foundation of Hunan Province of China (Grants No. 2022JJ20050, No. 2021JJ30784, and No. 2020JJ4104), and the Central South University Innovation-Driven Research Programme (Grant No. 2023CXQD036).

-
- [1] D. D. Stancil and A. Prabhakar, *Spin waves* (Springer, Berlin, 2009).
 - [2] A. Prabhakar and D. D. Stancil, *Spin waves: Theory and applications* (Springer, New York, 2009).
 - [3] S. Demokritov, B. Hillebrands, and A. Slavin, Brillouin light scattering studies of confined spin waves: linear and nonlinear confinement, *Phys. Rep.* **348**, 441 (2001).
 - [4] K. Uchida, J. Xiao, H. Adachi, J. Ohe, S. Takahashi, J. Ieda, T. Ota, Y. Kajiwara,

- H. Umezawa, H. Kawai, G. E. W. Bauer, S. Maekawa, and E. Saitoh, Spin seebeck insulator, *Nature Mater.* **9**, 894 (2010).
- [5] V. E. Demidov, S. Urazhdin, A. Anane, V. Cros, and S. O. Demokritov, Spin-orbit-torque magnonics, *J. Appl. Phys.* **127**, 170901 (2020).
- [6] A. V. Chumak, V. I. Vasyuchka, A. A. Serga, and B. Hillebrands, Magnon spintronics, *Nat. Phys.* **11**, 453 (2015).
- [7] A. V. Chumak, A. A. Serga, and B. Hillebrands, Magnon transistor for all-magnon data processing, *Nat. Commun.* **5**, 4700 (2014).
- [8] Q. Wang, P. Pirro, R. Verba, A. Slavin, B. Hillebrands, and A. V. Chumak, Reconfigurable nanoscale spin-wave directional coupler, *Sci. Adv.* **4**, e1701517 (2018).
- [9] Q. Wang, M. Kewenig, M. Schneider, R. Verba, F. Kohl, B. Heinz, M. Geilen, M. Mohseni, B. Lagel, F. Ciubotaru, C. Adelman, C. Dubs, S. D. Cotofana, O. V. Dobrovolskiy, T. Bracher, P. Pirro, and A. V. Chumak, A magnonic directional coupler for integrated magnonic half-adders, *Nat. Electron.* **3**, 765 (2020).
- [10] Y. Fan, P. Quarterman, J. Finley, J. Han, P. Zhang, J. T. Hou, M. D. Stiles, A. J. Grutter, and L. Liu, Manipulation of coupling and magnon transport in magnetic metal-insulator hybrid structures, *Phys. Rev. Appl.* **13**, 061002 (2020).
- [11] A. V. Sadovnikov, A. A. Grachev, V. A. Gubanov, S. A. Odintsov, A. A. Martyshkin, S. E. Sheshukova, Y. P. Sharaevskii, and S. A. Nikitov, Spin-wave intermodal coupling in the interconnection of magnonic units, *Appl. Phys. Lett.* **112**, 142402 (2018).
- [12] L. Liu, O. J. Lee, T. J. Gudmundsen, D. C. Ralph, and R. A. Buhrman, Current-induced switching of perpendicularly magnetized magnetic layers using spin torque from the spin hall effect, *Phys. Rev. Lett.* **109**, 096602 (2012).
- [13] K. Garello, I. M. Miron, C. O. Avci, F. Freimuth, Y. Mokrousov, S. Blugel, S. Auffret, O. Boulle, G. Gaudin, and P. Gambardella, Symmetry and magnitude of spin-orbit torques in ferromagnetic heterostructures, *Nat. Nanotechnol.* **8**, 587 (2013).
- [14] A. Hoffmann, Spin hall effects in metals, *IEEE Trans. Magn.* **49**, 5172 (2013).
- [15] X.-g. Wang, G.-h. Guo, and J. Berakdar, Steering magnonic dynamics and permeability at exceptional points in a parity-time symmetric waveguide, *Nat. Commun.* **11**, 5663 (2020).
- [16] T. Yu, H. Yang, L. Song, P. Yan, and Y. Cao, Higher-order exceptional points in ferromagnetic trilayers, *Phys. Rev. B* **101**, 144414 (2020).

- [17] X.-g. Wang, G.-h. Guo, and J. Berakdar, Enhanced sensitivity at magnetic high-order exceptional points and topological energy transfer in magnonic planar waveguides, [Phys. Rev. Appl. **15**, 034050 \(2021\)](#).
- [18] X.-G. Wang, G.-H. Guo, and J. Berakdar, Electric steering of spin excitation in nanostructured synthetic antiferromagnet, [Appl. Phys. Lett. **117**, 242406 \(2020\)](#).
- [19] X.-g. Wang, D. Schulz, G.-h. Guo, and J. Berakdar, Magnon dynamics in parity-time-symmetric dipolarly coupled waveguides and magnonic crystals, [Phys. Rev. Appl. **18**, 024080 \(2022\)](#).
- [20] C. M. Bender and S. Boettcher, Real spectra in non-hermitian hamiltonians having \mathcal{PT} symmetry, [Phys. Rev. Lett. **80**, 5243 \(1998\)](#).
- [21] C. M. Bender, D. C. Brody, and H. F. Jones, Complex extension of quantum mechanics, [Phys. Rev. Lett. **89**, 270401 \(2002\)](#).
- [22] C. M. Bender, Making sense of non-hermitian hamiltonians, [Rep. Prog. Phys. **70**, 947 \(2007\)](#).
- [23] L. Feng, Z. J. Wong, R.-M. Ma, Y. Wang, and X. Zhang, Single-mode laser by parity-time symmetry breaking, [Science **346**, 972 \(2014\)](#).
- [24] R. El-Ganainy, K. G. Makris, M. Khajavikhan, Z. H. Musslimani, S. Rotter, and D. N. Christodoulides, Non-hermitian physics and pt symmetry, [Nat. Phys. **14**, 11 \(2018\)](#).
- [25] C. E. Rüter, K. G. Makris, R. El-Ganainy, D. N. Christodoulides, M. Segev, and D. Kip, Observation of parity-time symmetry in optics, [Nat. Phys. **6**, 192 \(2010\)](#).
- [26] A. Regensburger, C. Bersch, M.-A. Miri, G. Onishchukov, D. N. Christodoulides, and U. Peschel, Parity-time synthetic photonic lattices, [Nature **488**, 167 \(2012\)](#).
- [27] M.-A. Miri and A. Alù, Exceptional points in optics and photonics, [Science **363**, eaar7709 \(2019\)](#).
- [28] X. Zhu, H. Ramezani, C. Shi, J. Zhu, and X. Zhang, \mathcal{PT} -symmetric acoustics, [Phys. Rev. X **4**, 031042 \(2014\)](#).
- [29] R. Fleury, D. Sounas, and A. Alù, An invisible acoustic sensor based on parity-time symmetry, [Nat. Commun. **6**, 5905 \(2015\)](#).
- [30] S. Assaworarith, X. Yu, and S. Fan, Robust wireless power transfer using a nonlinear parity-time-symmetric circuit, [Nature **546**, 387 \(2017\)](#).
- [31] P.-Y. Chen, M. Sakhdari, M. Hajizadegan, Q. Cui, M. M.-C. Cheng, R. El-Ganainy, and A. Alù, Generalized parity-time symmetry condition for enhanced sensor telemetry, [Nat. Elec-](#)

- tron. **1**, 297 (2018).
- [32] J. M. Lee, T. Kottos, and B. Shapiro, Macroscopic magnetic structures with balanced gain and loss, *Phys. Rev. B* **91**, 094416 (2015).
- [33] D. Zhang, X.-Q. Luo, Y.-P. Wang, T.-F. Li, and J. Q. You, Observation of the exceptional point in cavity magnon-polaritons, *Nat. Commun.* **8**, 1368 (2017).
- [34] H. Yang, C. Wang, T. Yu, Y. Cao, and P. Yan, Antiferromagnetism emerging in a ferromagnet with gain, *Phys. Rev. Lett.* **121**, 197201 (2018).
- [35] A. Galda and V. M. Vinokur, Exceptional points in classical spin dynamics, *Sci. Rep.* **9**, 17484 (2019).
- [36] H. Liu, D. Sun, C. Zhang, M. Groesbeck, R. Mclaughlin, and Z. V. Vardeny, Observation of exceptional points in magnonic parity-time symmetry devices, *Sci. Adv.* **5**, eaax9144 (2019).
- [37] C.-W. Sui, S.-H. Yuan, X.-G. Wang, J. Berakdar, and C. Jia, Emergent magnonic singularities in anti parity-time symmetric synthetic antiferromagnets, *New J. Phys.* **24**, 023031 (2022).
- [38] H. Hodaiei, A. U. Hassan, S. Wittek, H. Garcia-Gracia, R. El-Ganainy, D. N. Christodoulides, and M. Khajavikhan, Enhanced sensitivity at higher-order exceptional points, *Nature* **548**, 187 (2017).
- [39] J. Wiersig, Prospects and fundamental limits in exceptional point-based sensing, *Nat. Commun.* **11**, 2454 (2020).
- [40] J. Zhang, B. Peng, Ş. K. Özdemir, K. Pichler, D. O. Krimer, G. Zhao, F. Nori, Y.-x. Liu, S. Rotter, and L. Yang, A phonon laser operating at an exceptional point, *Nature Photon.* **12**, 479 (2018).
- [41] Y.-H. Lai, Y.-K. Lu, M.-G. Suh, Z. Yuan, and K. Vahala, Observation of the exceptional-point-enhanced sagnac effect, *Nature* **576**, 65 (2019).
- [42] J. Wiersig, Enhancing the sensitivity of frequency and energy splitting detection by using exceptional points: Application to microcavity sensors for single-particle detection, *Phys. Rev. Lett.* **112**, 203901 (2014).
- [43] A. V. Sadovnikov, A. A. Zyablovsky, A. V. Dorofeenko, and S. A. Nikitov, Exceptional-point phase transition in coupled magnonic waveguides, *Phys. Rev. Appl.* **18**, 024073 (2022).
- [44] M. Haidar, A. A. Awad, M. Dvornik, R. Khymyn, A. Houshang, and J. Åkerman, A single layer spin-orbit torque nano-oscillator, *Nature Commun.* **10**, 2362 (2019).
- [45] H. Fulara, M. Zahedinejad, R. Khymyn, A. A. Awad, S. Muralidhar, M. Dvornik, and

- J. Åkerman, Spin-orbit torque-driven propagating spin waves, *Sci. Adv.* **5**, eaax8467 (2019).
- [46] D. Houssameddine, U. Ebels, B. Delaët, B. Rodmacq, I. Firastrau, F. Ponthenier, M. Brunet, C. Thirion, J.-P. Michel, L. Prejbeanu-Buda, M.-C. Cyrille, O. Redon, and B. Dieny, Spin-torque oscillator using a perpendicular polarizer and a planar free layer, *Nature Mater.* **6**, 447 (2007).
- [47] S. Kaka, M. R. Pufall, W. H. Rippard, T. J. Silva, S. E. Russek, and J. A. Katine, Mutual phase-locking of microwave spin torque nano-oscillators, *Nature* **437**, 389 (2005).
- [48] S. P. Pati, Influence on the gilbert damping of yttrium-iron-garnet films by the spin-pumping effect, *Mater. Sci. Semicond. Process.* **107**, 104821 (2020).
- [49] C. Hauser, T. Richter, N. Homonnay, C. Eisenschmidt, M. Qaid, H. Deniz, D. Hesse, M. Sawicki, S. G. Ebbinghaus, and G. Schmidt, Yttrium iron garnet thin films with very low damping obtained by recrystallization of amorphous material, *Sci. Rep.* **6**, 20827 (2016).
- [50] See Supplemental Material at [URL will be inserted by publisher] for magnetization dynamics details, spatially-periodic gain/loss and loss/more-loss, and influences of damping and dipole-dipole interaction. which includes Refs. [8, 15, 43, 46, 47, 52–54].
- [51] D. M. Larsen and N. Bloembergen, Excitation of polyatomic molecules by radiation, *Opt. Commun.* **17**, 254 (1976).
- [52] R. Verba, G. Melkov, V. Tiberkevich, and A. Slavin, Collective spin-wave excitations in a two-dimensional array of coupled magnetic nanodots, *Phys. Rev. B* **85**, 014427 (2012).
- [53] M. Beleggia, S. Tandon, Y. Zhu, and M. D. Graef, On the magnetostatic interactions between nanoparticles of arbitrary shape, *J. Magn. Magn. Mater.* **278**, 270 (2004).
- [54] X.-g. Wang, L. Chotorlishvili, G.-h. Guo, and J. Berakdar, High-fidelity magnonic gates for surface spin waves, *Phys. Rev. Appl.* **12**, 034015 (2019).